



HAL
open science

Nonlinear primal–dual algorithm for the phase and absorption retrieval from a single phase contrast image

Kannara Mom, Max Langer, Bruno Sixou

► **To cite this version:**

Kannara Mom, Max Langer, Bruno Sixou. Nonlinear primal–dual algorithm for the phase and absorption retrieval from a single phase contrast image. *Optics Letters*, 2022, 47 (20), pp.5389. 10.1364/OL.469174 . hal-03839399

HAL Id: hal-03839399

<https://hal.science/hal-03839399>

Submitted on 4 Nov 2022

HAL is a multi-disciplinary open access archive for the deposit and dissemination of scientific research documents, whether they are published or not. The documents may come from teaching and research institutions in France or abroad, or from public or private research centers.

L'archive ouverte pluridisciplinaire **HAL**, est destinée au dépôt et à la diffusion de documents scientifiques de niveau recherche, publiés ou non, émanant des établissements d'enseignement et de recherche français ou étrangers, des laboratoires publics ou privés.

Nonlinear primal-dual algorithm for phase and absorption retrieval from a single phase contrast image

KANNARA MOM^{1,*}, MAX LANGER², AND BRUNO SIXOU¹

¹Univ Lyon, INSA-Lyon, Université Claude Bernard Lyon 1, UJM-Saint Etienne, CNRS, Inserm, CREATIS UMR 5220, U1206, F-69621 Villeurbanne, France

²Univ. Grenoble Alpes, CNRS, UMR 5525, VetAgro Sup, Grenoble INP, TIMC, F-38000 Grenoble, France

*kannara.mom@creatis.insa-lyon.fr

Compiled November 4, 2022

We propose a non-linear primal-dual algorithm for the retrieval of phase shift and absorption from a single X-ray in-line phase contrast, or Fresnel diffraction, image. The algorithm permit to regularize phase and absorption separately. We demonstrate that taking into account the non-linearity in the reconstruction improves reconstruction compared to linear methods. We also demonstrate that choosing different regularizers for absorption and phase can improve the reconstructions. The use of the Total Variation and its generalization in a primal-dual approach allows to exploit the sparsity of the investigated sample. On both simulated and real datasets, the proposed NL-PDHG method yields reconstructions with considerably less artifacts and improved the normalized mean squared error compared to its linearized version.

© 2022 Optica Publishing Group

<http://dx.doi.org/10.1364/ao.XX.XXXXXX>

Phase based X-ray imaging techniques have seen significant development recently due to the high sensitivity offered by phase contrast imaging [1], which has several applications in material science [2] and biomedical imaging [3, 4]. When using sufficiently coherent X-ray beams, phase contrast can be achieved by letting the wave propagate in free space after interaction with the sample [5]. Using relatively short distance, the relationship between the absorption and phase shift induced by a sample and the diffraction pattern relies on the Fresnel diffraction theory. The phase information is lost and must be estimated from one or several of those diffraction patterns. Phase retrieval in this context is a non-linear ill-posed inverse problem. The single-distance problem, i.e. using a single image, is known to be more severely ill-posed than the classical problems with several diffraction patterns [6, 7].

Solving this problem is non-trivial, therefore, several phase retrieval methods have been proposed to find suitable solutions. Direct inversion methods are based on the linearization of the forward model. These include the Transport of Intensity Equation (TIE) [8], Contrast Transfer Function (CTF) [9] and the Mixed approach [10]. Such analytical approaches are only valid under some assumptions on the imaging conditions, e.g., a homogeneous object or relatively short propagation distance.

Iterative methods are generally not limited by these constraints. Several iterative schemes have been proposed, either based on alternating projections on constraints imposed by the measured intensities and some prior knowledge in the object space [11] or variational methods which consist in minimizing a functional. Among these, we have the methods based on the Fréchet derivative of the forward operator in conjunction with the Landweber algorithm. This kind of algorithm enables a flexible inclusion of priors, such as Tikhonov or sparsity regularization [12]. A regularized Newton method that can address any specific kind of phase retrieval problem has also been introduced [13]. In order to include prior such as the Total Variation (TV), primal-dual schemes like Alternating Direction Method of Multipliers (ADMM) have been studied for the phase retrieval problem but rely on linearization of the forward model, either using TIE [14] or CTF [15]. Few of the methods mentioned above propose to treat the single-distance problem without any assumption on the object composition or on the support of the object.

More recently, data-driven methods based on neural networks have been investigated. Several architectures have been proposed for the phase retrieval problem, the Mixed Scale Dense Networks [16] was trained in a supervised manner to retrieve absorption and phase from the diffraction patterns without any other information. The PhaseGAN [17] was trained in an unsupervised way, while taking into account the effect of the propagator. Both were able to retrieve the absorption and the phase from a single diffraction pattern. Although data-driven methods have yielded very good reconstructions, they often require a large database and the reconstruction quality is limited by the quality of the training data.

In this work, we present a primal-dual approach based on the primal-dual hybrid gradient (PDHG) method [18] that can retrieve both the absorption and the phase with a single noisy diffraction pattern without homogeneity assumption or support constraint. We first propose an iterative method for the linearized CTF problem and then generalize it to the nonlinear case. We exploit the possibility to use different priors for absorption and phase to take into account the specificities of each quantity. Experiments performed on simulated and real data acquired show that working with Total Variation (TV) [19] and Total Generalized Variation of second order (TGV²) [20] visually improves the quality of the retrieved piecewise constant maps.

For thin objects and straight-line propagation of the beam

along the propagation direction z , the interaction of coherent and parallel X-ray beam with matter can be described by a transmittance function [8]. Assuming plane wave illumination, the intensity measured at a distance D downstream of the object is given by the squared module of the convolution between the transmittance function and the Fresnel propagator. The forward model describing the nonlinear relationship between the absorption B and phase shift φ induced by a sample and the diffraction pattern can thus be written as

$$\mathbf{F}_D(B, \varphi) = |e^{-B+i\varphi} * P_D|^2 \quad (1)$$

where $P_D(\cdot) = \frac{1}{i\lambda D} \exp(i\frac{\pi}{\lambda D} |\cdot|^2)$ is the Fresnel propagator. Estimating the phase shift and the absorption from the intensity, or diffraction pattern, is called phase (and absorption) retrieval. The CTF [9] gives an approximation of the measured intensity at the detector, thus obtaining a linear relationship between intensity and phase, which is valid for weak absorption and slowly varying phase shift. For compactness, we can write the CTF as

$$\mathbf{F}_D^{\text{CTF}}(B, \varphi) = 2 \left\{ \mathcal{F}^{-1} [-\cos(\alpha_D), \sin(\alpha_D)] \mathcal{F} \right\} (B, \varphi) \quad (2)$$

with $\alpha_D = \pi\lambda D |f|^2$, where f denotes the coordinates in the Fourier domain. The CTF can retrieve a quantitative solution of B and φ , but several distances have to be used in order to cover as much of the Fourier domain as possible.

Different approaches have been proposed to recover both the phase and absorption from a single distance [7, 12], but none of them proposed the use of prior such as the TV regularization while taking into account the nonlinearity. Previous works on phase retrieval showed that TV regularization improves the quality of the retrieved piecewise constant phase maps, but they only treated the linear case [14, 15]. To solve the non-linear problem with TV regularization, we propose an approach based on the PDHG method [18], which allows the use of TV regularization as well as its second order generalization (TGV²). The PDHG has been generalized to nonlinear settings in order to use nonlinear operators [21]. We then derive two algorithms, one based on CTF-linearization (PDHG-CTF) and a more general one, the nonlinear primal-dual hybrid gradient (NL-PDHG). Following [22], we observe that instead of defining a regularization on the complex-valued function $f = -B + i\varphi$ as in [7], since the contribution of attenuation and phase to the phase contrast image is different, it may be more interesting to use different regularization for B and φ respectively.

Choosing the weighting parameters to be $\alpha, \beta, \nu > 0$, we then seek to solve the following minimization problem:

$$\min_{\substack{B, \varphi \\ B > 0, \varphi > 0}} \left\{ \left\| \mathbf{F}_D^{\text{CTF}}(B, \varphi) - \mathbf{I}_D^{\text{obs}} \right\|_2^2 + \text{TGV}_{(\alpha, \beta)}^2(B) + \nu \text{TV}(\varphi) \right\} \quad (3)$$

where $\mathbf{I}_D^{\text{obs}}$ is a noisy measured intensity at a distance D . The Total Variation is defined as $\text{TV}(\varphi) = \|(\nabla\varphi)_x\|_1 + \|(\nabla\varphi)_y\|_1$, where ∇ is the discrete gradient operator, and the TGV² can be formulated as follows [23]:

$$\text{TGV}_{(\alpha, \beta)}^2(B) = \min_{\mathbf{v}} \{ \alpha \|\mathfrak{D}\mathbf{v}\|_1 + \beta \|\nabla B - \mathbf{v}\|_1 \} \quad (4)$$

where $\mathbf{v} = (v_1, v_2)$ is an auxiliary variable and $\mathfrak{D}(\mathbf{v}) = \frac{\nabla v_1 + \nabla v_2}{2}$. One can see how the α parameter forces \mathbf{v} to have a sparse gradient and the β parameter penalizes the gradient ∇B to deviate only on a sparse set from \mathbf{v} . The minimization problem Eq. (3) can be rewritten as:

$$\min_{B, \varphi, \mathbf{v}} \{ \mathcal{H}[K(B, \varphi, \mathbf{v})] + \mathcal{G}(B, \varphi, \mathbf{v}) \} \quad (5)$$

Algorithm 1. PDHG-CTF

- σ_0, τ_0 such that $\sigma_0\tau_0\|\mathcal{K}\|^2 < 1$, $\gamma \in [0, 1]$ and N_{iter} .
 - initial guesses $x_0 = (B_0, \varphi_0, \mathbf{v}_0)$ and $h_0 = (h_0^1, h_0^2, h_0^3, h_0^4)$
- for $i = 0, \dots, N_{\text{iter}}$ do:
- $$h_{i+1} \leftarrow \text{prox}_{\sigma_i \mathcal{H}^*} (h_i + \sigma_i \mathcal{K} \bar{x}_i)$$
- $$x_{i+1} \leftarrow \text{prox}_{\tau_i \mathcal{G}} (x_i - \tau_i \mathcal{K}^* h_{i+1})$$
- $$\bar{x}_{i+1} \leftarrow x_{i+1} + \gamma (x_{i+1} - x_i)$$

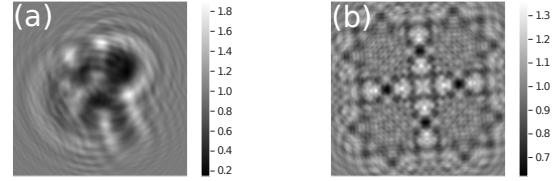


Fig. 1. (a) Simulated intensity with Gaussian noise. (b) Experimental intensity acquired at beamline NanoMAX.

with

$$\mathcal{K}(B, \varphi, \mathbf{v}) = \left[\mathbf{F}_D^{\text{CTF}}(B, \varphi), \mathfrak{D}(\mathbf{v}), \nabla B - \mathbf{v}, \nabla \varphi \right] \quad (6)$$

$$\mathcal{H}(h^1, h^2, h^3, h^4) = \|h^1 - \mathbf{I}_D^{\text{obs}}\|_2^2 + \alpha \|h^2\|_1 + \beta \|h^3\|_1 + \nu \|h^4\|_1 \quad (7)$$

Here \mathcal{K} is a linear operator, and $\mathcal{G} = \chi_{>0}$ is an indicator function, it forces B and φ to be positive. Using this formulation, we define the PDHG-CTF algorithm (Alg. 1), which iterates over the triplet $x_i = (B_i, \varphi_i, \mathbf{v}_i)$, where B_i and φ_i represent the absorption and phase shift we are looking for, and \mathbf{v}_i is the variable from the formula for TGV (Eq. (4)), at the i -th iteration. Here, τ_i and σ_i are the step sizes of the primal and dual space, respectively, \mathcal{K}^* denotes the adjoint operator of \mathcal{K} , $\text{prox}_{\tau_i \mathcal{G}}$ the proximal operator of $\tau_i \mathcal{G}$ and \mathcal{H}^* the conjugate of \mathcal{H} . To ensure convergence [18] of algorithm 1, we can simply choose fixed step sizes σ, τ , e.g., $\sigma_i = \sigma$ and $\tau_i = \tau$ for all i , as long as $\sigma\tau\|\mathcal{K}\|^2 < 1$, where $\|\mathcal{K}\|$ is the operator norm. Originally designed for linear operator, the PDHG algorithm has been generalized to nonlinear cases [21]. By replacing the linear operator $\mathbf{F}_D^{\text{CTF}}$ (Eq. (2)) by the nonlinear operator \mathbf{F}_D (Eq. (1)) in the problem Eq. (3), we obtain a new minimization problem that we can solve with the NL-PDHG method. The only change from PDHG-CTF (Alg. 1) is that the operator \mathcal{K} is now nonlinear, in this case \mathcal{K}^* has to be replaced by $[\mathcal{K}'(x_i)]^*$ where $\mathcal{K}'(x_i)$ is the Fréchet derivative at the point x_i , for which we have an explicit formula [12]. In order to ensure the convergence of the algorithm, the gradient of \mathcal{K} has to be Lipschitz in a neighborhood of a solution, the initial iterate has to be close enough to a solution and the step sizes must satisfy the local inequalities [21]: $\sigma_i \tau_i \sup_{k=0,1,\dots,i} \{ \|\mathcal{K}'(x_k)\|^2 \} < 1$.

In order to evaluate the algorithms, a set of 3D object were generated by creating random combinations of one to ten ellipsoid or paraboloid shapes consisting of three different materials: gold (Au), palladium (Pd) and zinc (Zn). 2D projections of size 512×512 pixels were generated, yielding images of the phase and the absorption, which were subsequently used to generate phase contrast images (Fig. 1) by using Eq. (1). The X-ray energy was set to 13 keV for a wavelength of $\lambda = 0.095$ nm, the propagation distance $D = 10$ mm and the pixel size to 24 nm. As quantitative measures of reconstruction quality and to quantify the uncertainty of the reconstructions we generated a test dataset of 1000 images to compare the methods. For comparison, we used a projected gradient descent regularized with

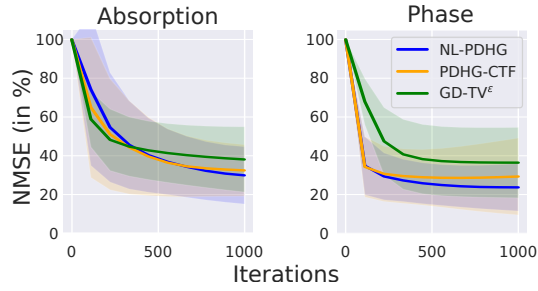


Fig. 2. Evolution of average NMSE (%) of the different methods for 1000 test images. The transparent areas correspond to the standard deviation.

smooth total variation (TV^ϵ) [24], dubbed $GD-TV^\epsilon$, where ϵ is a smoothing factor. The parameters for the different methods have been optimized by scanning in a wide interval to obtain a large decrease of the data term. For $GD-TV^\epsilon$, the smoothing factor was set to 10^{-3} , with different weighting parameters for B and φ , equal to 10^{-1} and 10^{-3} , respectively. For both PDHG-CTF and NL-PDHG, we used the same set of parameters: $\alpha = 10^{-2}$, $\beta = 5 \times 10^{-3}$, $\nu = 10^{-2}$ and the relaxation parameter $\gamma = 1$. A stopping criterion based on the pseudo-duality gap has been proposed, [21], but its calculation is expensive computationally. Therefore, we used a fixed number of iterations ($N_{iter} = 1000$) which was sufficient to achieve convergence (Fig. 2). While theoretically, the initialization must be close enough to a solution to ensure convergence, in practice, the algorithm converged when initializing with $(B_0, \varphi_0) = (0, 0)$. In the following, the algorithm is always initialized at zero. For $GD-TV^\epsilon$, convergence was not analyzed in detail, but a sufficiently small fixed step size of 0.01 was enough to obtain convergence of the iterates in practice. For PDHG-CTF, setting the step sizes to $\sigma = \tau = 0.99 \|\mathcal{K}\|^{-1}$ ensured convergence in all cases. And for NL-PDHG, the step sizes were set to $\sigma_i = \tau_i = 0.99L_i$, where $L_i = \sup_{k=0,1,\dots,i} \{\|\mathcal{K}'(x_k)\|^2\}$, and they were update every 50 iterations, in order to satisfy the local inequalities. The methods was implemented in Python on a Intel(R) Core(TM) i7-10610U CPU at 1.80 GHz [25]. It took about 104 s for $GD-TV^\epsilon$ and 120 s for both PDHG-CTF and NL-PDHG methods.

Reconstructed phase and absorption projections using a simulated object are displayed in Fig. 3. The $GD-TV^\epsilon$ algorithm yielded the lowest quality reconstruction. Parts of the object are missing, possibly caused by the projection on positive values and the smooth approximation of TV. The PDHG-CTF method yielded somewhat better reconstructions, the main artefacts coming from the rather high attenuation induced by the object so that the weak attenuation and slowly varying phase assumptions of the CTF are not satisfied. As for NL-PDHG, the reconstructions present a clear visual improvement at the contour level, in particular, the fringes on the edges of materials are no longer present for the absorption compared to the linearized method. For quantitative analysis, we computed the average normalized mean squared error (NMSE), the structural similarity (SSIM) and the peak SNR (PSNR) on the test dataset, the results are summarized in Tab. 1. The primal-dual approaches perform better than the gradient descent, and overall the NL-PDHG method has the best reconstructions on average. We can see that applying the same regularization to B and φ gives worse reconstructions, and that the absorption is better recovered with a TGV^2 regularization while the phase has better results for the TV regularization. This can be explained by the fact that in our experiments, the

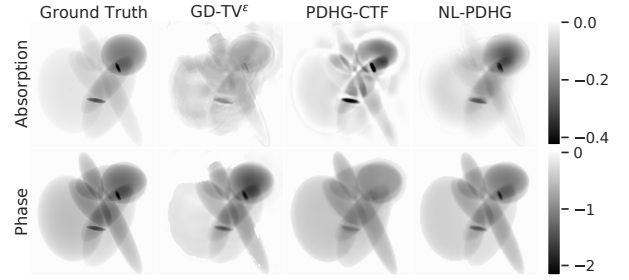


Fig. 3. Reconstructions from the simulated intensity.

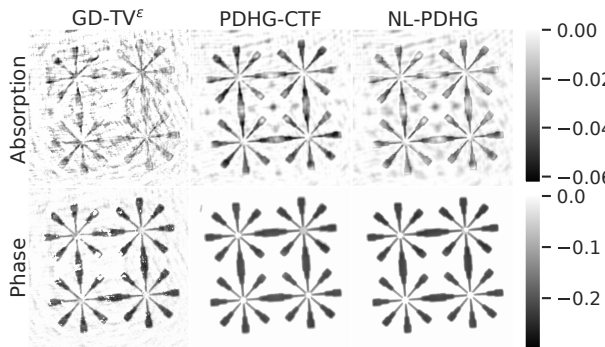
retrieved absorption tends to have missing parts which, when reconstructed with TV leaves some staircasing effects. Using TGV^2 regularization for B offers best performance, providing a good compromise between sharp boundaries and smoothness. While for φ , a better reconstruction cannot be expected by taking into account the second order. Moreover, if the considered objects has sufficiently weak attenuation and slowly varying phase, then the PDHG-CTF method converges faster. It needs a hundred iterations to obtain the same quality of reconstruction on average as the nonlinear version, which needs a thousand iterations. In contrast, if we consider the most absorbent object of the dataset, which has a maximum absorption equal to 0.882. Then the CTF approximation is less good and the linearized method gives a NMSE of 60.5 and 75.7 while NL-PDHG gives a NMSE of 47.9 and 61.4 for the absorption and phase, respectively.

To demonstrate the capability of this primal-dual framework, the methods were applied on experimental data acquired at beamline NanoMAX at the MAX IV synchrotron (Lund, Sweden) [26]. The diffraction pattern (2048×2048 pixels) in Fig. 1 was obtained with an effective pixel size of 6 nm and a defocusing distance $D = 20$ mm. The X-ray energy was set to 13 keV for a wavelength of $\lambda = 0.095$ nm. The sample consists of a stack of Pd, Zn, Pd, Au metal layers with thicknesses of 21, 10, 11, 163 nm, respectively, deposited on a 1 mm-thick silicon nitride substrate, thus the expected values for absorption and phase are 0.0483 and 0.217. The execution time was 37 min for $GD-TV^\epsilon$ and 50 min for the primal-dual methods, after 1000 iterations. As shown in Fig. 4, the $GD-TV^\epsilon$ algorithm yields the same problems of missing parts of the object as on simulated data in the recovered phase and absorption. Both primal-dual approaches seem to retrieve well the absorption, while reducing spurious fringes in the background, and the recovered phases are close to artifact-free. Note that here the object is not very absorbing since it is quite thin. Therefore, the linearized method also yields a very good reconstruction. And since the object is piecewise constant, TV and TGV type regularizations are well suited.

We presented two algorithms based on a primal-dual approach for the reconstruction of both the absorption and phase from a single diffraction pattern. The algorithms permit the use of different regularizations for absorption and phase, which was shown to improve reconstructions by selecting regularizations that take into account the way the attenuation and phase contributes to the phase contrast image. In addition, we observed the significant contribution of the nonlinear information of the problem, this suggests that the NL-PDHG algorithm could be applied in a wide variety of cases where linear methods would fail. A drawback of the algorithms is that three regularization parameters must be chosen. The choice of parameters was shown to be robust by application to a large set of images, however. The method could be used for samples that have higher phase over

Table 1. Average NMSE, SSIM, PSNR and standard deviation for 1 000 test images using different strategies for regularization.

	Regularization		NMSE (in %)		SSIM (in %)		PSNR	
	Absorption	Phase	Absorption	Phase	Absorption	Phase	Absorption	Phase
GD-TV ^e	TV ^e	TV ^e	37.5 (17.4)	36.4 (18.2)	99.6 (0.440)	95.2 (6.95)	65.2 (9.43)	50.5 (11.1)
PDHG-CTF	TGV ²	TV	32.1 (12.9)	29.6 (20.9)	99.8 (0.337)	92.9 (7.87)	68.2 (9.10)	52.6 (8.19)
NL-PDHG	TGV ²	TV	29.2 (14.8)	23.6 (12.6)	99.8 (0.237)	97.2 (3.12)	68.7 (8.63)	53.0 (6.40)
NL-PDHG	TV	TV	41.3 (23.9)	25.6 (14.1)	99.7 (0.371)	94.8 (5.10)	65.0 (9.72)	52.8 (7.53)
NL-PDHG	TGV ²	TGV ²	32.4 (19.6)	29.3 (14.8)	99.8 (0.249)	92.3 (6.58)	66.8 (8.00)	51.4 (6.51)

**Fig. 4.** Reconstructions from the experimental intensity.

absorption ratio [27] or have more complex structures by adjusting the parameters and increasing the number of iterations, but further investigation should be carried out for non-sparse objects, such as those encountered in biological soft-tissue imaging. The case of X-rays from a laboratory environment can be studied by considering the Kullback-Leibler divergence instead of l_2 norm. A direct extension of this work would be to apply the proposed algorithms to phase contrast tomography [28], in particular when there is no assumption of multi-materials, considering the 3D version of TV or generalized TV. Finally, the algorithms could be extended by using neural networks to learn the regularization parameters or the regularization itself.

Acknowledgments. We acknowledge Pablo Villanueva-Perez (Lund University, Lund, Sweden) and Sebastian Kalbfleisch (MAX IV Laboratory, Lund, Sweden) for the acquisition of the experimental data, and Jesper Wallentin and Lert Chayanun (NanoLund and Lund University, Lund, Sweden) for the sample.

Disclosures. The authors declare no conflicts of interest.

Data Availability Statement. Data underlying the simulated results can be generated using *TomoPhantom* software [29]. Data underlying the experimental results are available through the *PyPhase* package [30].

REFERENCES

1. A. Momose, T. Takeda, Y. Itai, and K. Hirano, *Nat. Med.* **2**, 473 (1996).
2. S. C. Mayo, A. W. Stevenson, and S. W. Wilkins, *Materials* **5**, 937 (2012).
3. M. Langer, A. Pacureanu, H. Suhonen, Q. Grimal, P. Cloetens, and F. Peyrin, *PLOS ONE* **7**, 1 (2012).
4. A. Giuliani, S. Mazzoni, L. Mele, D. Liccardo, G. Tromba, and M. Langer, *Front. Physiol.* **8** (2017).
5. P. Cloetens, R. Barrett, J. Baruchel, J.-P. Guigay, and M. Schlenker, *J. Phys. D: Appl. Phys.* **29**, 133 (1996).
6. M. Beleggia, M. Schofield, V. Volkov, and Y. Zhu, *Ultramicroscopy* **102**, 37 (2004).
7. S. Maretzke and T. Hohage, *SIAM J. on Appl. Math.* **77**, 384 (2017).
8. Paganin, *Coherent X-ray optics* (Oxford University Press, 2006).

9. P. Cloetens, W. Ludwig, J. Baruchel, D. Van Dyck, J. Van Landuyt, J. P. Guigay, and M. Schlenker, *Appl. Phys. Lett.* **75**, 2912 (1999).
10. J. P. Guigay, M. Langer, R. Boistel, and P. Cloetens, *Opt. Lett.* **32**, 1617 (2007).
11. R. W. Gerchberg and W. O. Saxton, *Optik* **35**, 237 (1972).
12. B. Sixou, V. Davidoiu, M. Langer, and F. Peyrin, *Inverse Probl. Imaging* **7**, 267 (2013).
13. S. Maretzke, M. Bartels, M. Krenkel, T. Salditt, and T. Hohage, *Opt. Express* **24**, 6490 (2016).
14. E. Bostan, E. Froustey, B. Rappaz, E. Shaffer, D. Sage, and M. A. Unser, *IEEE ICIP* **2014**, 3939 (2014).
15. P. Villanueva-Perez, F. Arcadu, P. Cloetens, and M. Stampanoni, *Opt. Lett.* **42**, 1133 (2017).
16. K. Mom, B. Sixou, and M. Langer, *Appl. Opt.* **61**, 2497 (2022).
17. Y. Zhang, M. A. Noack, P. Vagovic, K. Fezzaa, F. Garcia-Moreno, T. Rietschel, and P. Villanueva-Perez, *Opt. Express* **29**, 19593 (2021).
18. A. Chambolle and T. Pock, *J. Math. Imaging Vis.* **40**, 120 (2011).
19. L. I. Rudin, S. Osher, and E. Fatemi, *Phys. D* **60**, 259 (1992).
20. K. Bredies, K. Kunisch, and T. Pock, *SIAM J. Imag. Sci.* **3**, 492 (2010).
21. T. Valkonen, *Inverse Probl.* **30**, 055012 (2014).
22. T. Valkonen, K. Bredies, and F. Knoll, *SIAM J. Imag. Sci.* **6**, 487 (2013).
23. A. Chambolle and T. Pock, *Acta Numer.* **25**, 161–319 (2016).
24. E. M. Kalmoun, *J. Imaging* **4** (2018).
25. M. Langer, <https://doi.org/10.5281/zenodo.4623696> (2021).
26. S. Kalbfleisch, Y. Zhang, M. Kahnt, K. Buakor, M. Langer, T. Dreier, H. Dierks, P. Stjärneblad, E. Larsson, K. Gordeyeva, L. Chayanun, D. Söderberg, J. Wallentin, M. Bech, and P. Villanueva-Perez, *J. Synchrotron Radiat.* **29**, 224 (2022).
27. S. J. Alloo, D. M. Paganin, K. S. Morgan, T. E. Gureyev, S. C. Mayo, S. Mohammadi, D. Lockie, R. H. Menk, F. Arfelli, F. Zanconati, G. Tromba, and K. M. Pavlov, *Opt. Lett.* **47**, 1945 (2022).
28. A. Kostenko, K. J. Batenburg, A. King, S. E. Offerman, and L. J. van Vliet, *Opt. Express* **21**, 12185 (2013).
29. D. Kazantsev, V. Pickalov, S. Nagella, P. Edoardo, and P. J. Withers, *SoftwareX* **7**, 150 (2018).
30. M. Langer, Y. Zhang, D. Figueirinhas, J.-B. Forien, K. Mom, C. Mouton, R. Mokso, and P. Villanueva-Perez, *J. Synchrotron Radiat.* **28**, 1261 (2021).

FULL REFERENCES

- 330
331 1. A. Momose, T. Takeda, Y. Itai, and K. Hirano, "Phase-contrast x-ray
332 computed tomography for observing biological soft tissues," *Nat. Med.*
333 **2**, 473–475 (1996).
334 2. S. C. Mayo, A. W. Stevenson, and S. W. Wilkins, "In-line phase-contrast
335 x-ray imaging and tomography for materials science," *Materials* **5**, 937
336 – 965 (2012).
337 3. M. Langer, A. Pacureanu, H. Suhonen, Q. Grimal, P. Cloetens, and
338 F. Peyrin, "X-ray phase nanotomography resolves the 3d human bone
339 ultrastructure," *PLOS ONE* **7**, 1–7 (2012).
340 4. A. Giuliani, S. Mazzoni, L. Mele, D. Liccardo, G. Tromba, and M. Langer,
341 "Synchrotron phase tomography: An emerging imaging method for
342 microvessel detection in engineered bone of craniofacial districts," *Front.*
343 *Physiol.* **8** (2017).
344 5. P. Cloetens, R. Barrett, J. Baruchel, J.-P. Guigay, and M. Schlenker,
345 "Phase objects in synchrotron radiation hard x-ray imaging," *J. Phys. D:*
346 *Appl. Phys.* **29**, 133–146 (1996).
347 6. M. Beleggia, M. Schofield, V. Volkov, and Y. Zhu, "On the transport of
348 intensity technique for phase retrieval," *Ultramicroscopy* **102**, 37–49
349 (2004).
350 7. S. Maretzke and T. Hohage, "Stability estimates for linearized near-field
351 phase retrieval in x-ray phase contrast imaging," *SIAM J. on Appl. Math.*
352 **77**, 384–408 (2017).
353 8. Paganin, *Coherent X-ray optics* (Oxford University Press, 2006).
354 9. P. Cloetens, W. Ludwig, J. Baruchel, D. Van Dyck, J. Van Landuyt, J. P.
355 Guigay, and M. Schlenker, "Holotomography: Quantitative phase to-
356 mography with micrometer resolution using hard synchrotron radiation
357 x rays," *Appl. Phys. Lett.* **75**, 2912–2914 (1999).
358 10. J. P. Guigay, M. Langer, R. Boistel, and P. Cloetens, "Mixed transfer
359 function and transport of intensity approach for phase retrieval in the
360 fresnel region," *Opt. Lett.* **32**, 1617–1619 (2007).
361 11. R. W. Gerchberg and W. O. Saxton, "A practical algorithm for the
362 determination of phase from image and diffraction plane pictures,"
363 *Optik* **35**, 237–246 (1972).
364 12. B. Sixou, V. Davidoiu, M. Langer, and F. Peyrin, "Absorption and phase
365 retrieval with tikhonov and joint sparsity regularizations," *Inverse Probl.*
366 *Imaging* **7**, 267–282 (2013).
367 13. S. Maretzke, M. Bartels, M. Krenkel, T. Salditt, and T. Hohage, "Regu-
368 larized newton methods for x-ray phase contrast and general imaging
369 problems," *Opt. Express* **24**, 6490–6506 (2016).
370 14. E. Bostan, E. Froustey, B. Rappaz, E. Shaffer, D. Sage, and M. A.
371 Unser, "Phase retrieval by using transport-of-intensity equation and
372 differential interference contrast microscopy," *IEEE ICIP* **2014**, 3939
373 (2014).
374 15. P. Villanueva-Perez, F. Arcadu, P. Cloetens, and M. Stampanoni,
375 "Contrast-transfer-function phase retrieval based on compressed sens-
376 ing," *Opt. Lett.* **42**, 1133–1136 (2017).
377 16. K. Mom, B. Sixou, and M. Langer, "Mixed scale dense convolutional
378 networks for x-ray phase contrast imaging," *Appl. Opt.* **61**, 2497–2505
379 (2022).
380 17. Y. Zhang, M. A. Noack, P. Vagovic, K. Fezzaa, F. Garcia-Moreno,
381 T. Ritschel, and P. Villanueva-Perez, "PhaseGAN: a deep-learning
382 phase-retrieval approach for unpaired datasets," *Opt. Express* **29**,
383 19593–19604 (2021).
384 18. A. Chambolle and T. Pock, "A first-order primal-dual algorithm for
385 convex problems with applications to imaging," *J. Math. Imaging Vis.*
386 **40**, 120–145 (2011).
387 19. L. I. Rudin, S. Osher, and E. Fatemi, "Nonlinear total variation based
388 noise removal algorithms," *Phys. D* **60**, 259–268 (1992).
389 20. K. Bredies, K. Kunisch, and T. Pock, "Total generalized variation," *SIAM*
390 *J. Imag. Sci.* **3**, 492–526 (2010).
391 21. T. Valkonen, "A primal–dual hybrid gradient method for nonlinear oper-
392 ators with applications to MRI," *Inverse Probl.* **30**, 055012 (2014).
393 22. T. Valkonen, K. Bredies, and F. Knoll, "Total generalized variation in
394 diffusion tensor imaging," *SIAM J. Imag. Sci.* **6**, 487–525 (2013).
395 23. A. Chambolle and T. Pock, "An introduction to continuous optimization
396 for imaging," *Acta Numer.* **25**, 161–319 (2016).
397 24. E. M. Kalmoun, "An investigation of smooth tv-like regularization in the
context of the optical flow problem," *J. Imaging* **4** (2018).
398
399 25. M. Langer, "PyPhase-1.0.1 : An open source phase retrieval code,"
400 <https://doi.org/10.5281/zenodo.4623696> (2021).
401 26. S. Kalbfleisch, Y. Zhang, M. Kahnt, K. Buakor, M. Langer, T. Dreier,
402 H. Dierks, P. Stjärneblad, E. Larsson, K. Gordeyeva, L. Chayanun,
403 D. Söderberg, J. Wallentin, M. Bech, and P. Villanueva-Perez, "X-ray
404 in-line holography and holotomography at the NanoMAX beamline," *J.*
405 *Synchrotron Radiat.* **29**, 224–229 (2022).
406 27. S. J. Alloo, D. M. Paganin, K. S. Morgan, T. E. Gureyev, S. C.
407 Mayo, S. Mohammadi, D. Lockie, R. H. Menk, F. Arfelli, F. Zanconati,
408 G. Tromba, and K. M. Pavlov, "Tomographic phase and attenuation
409 extraction for a sample composed of unknown materials using x-ray
410 propagation-based phase-contrast imaging," *Opt. Lett.* **47**, 1945–1948
411 (2022).
412 28. A. Kostenko, K. J. Batenburg, A. King, S. E. Offerman, and L. J. van
413 Vliet, "Total variation minimization approach in in-line x-ray phase-
414 contrast tomography," *Opt. Express* **21**, 12185–12196 (2013).
415 29. D. Kazantsev, V. Pickalov, S. Nagella, P. Edoardo, and P. J. Withers,
416 "TomPhantom, a software package to generate 2D–4D analytical phan-
417 toms for CT image reconstruction algorithm benchmarks," *SoftwareX*
418 **7**, 150–155 (2018).
419 30. M. Langer, Y. Zhang, D. Figueirinhas, J.-B. Forien, K. Mom, C. Mouton,
420 R. Mokso, and P. Villanueva-Perez, "PyPhase – a Python package for
421 X-ray phase imaging," *J. Synchrotron Radiat.* **28**, 1261–1266 (2021).